NOAA Technical Report NESDIS 75

DETECTION AND ANALYSIS OF FOG AT NIGHT USING GOES MULTISPECTRAL INFRARED IMAGERY

Washington, D.C.
January 1994

U.S. DEPARTMENT OF COMMERCE
National Oceanic and Atmospheric Administration
National Environmental Satellite, Data, and Information Service

NOAA TECHNICAL REPORTS

National Environmental Satellite, Data, and Information Service

nvironmental Satellite, Data, and Information Service (NESDIS) manages the Nation's civil Earth-systems, as well as global national data bases for meteorology, oceanography, geophysics, and solar-. From these sources, it develops and disseminates environmental data and information products ction of life and property, national defence, the national economy, energy development and distribution, global food supplies, and the development of natural resources.

Publication in the NOAA Technical Report series does not preclude later publication in scientific journals in expanded or modified form. The NESDIS series of NOAA Technical Reports is a continuation of the former NESS and EDIS series of NOAA Technical Reports and the NESC and EDS series of Environmental Science Services Administration (ESSA) Technical Reports.

A limited number of copies are available by contacting Nancy Everson, NOAA/NESDIS, E/RA22, 5200 Auth Road, Washington D.C., 20233. Copies can also be ordered from the National Technical Information Service (NTIS), U.S. Department of Commerce, Sills Bldg., 5285 Port Royal Road, Springfield, VA. 22161, (703) 487-4650 (prices on request for paper copies or microfiche, please refer to PB number when ordering). A partial listing of more recent reports appear below:

NESDIS 20 An Atlas of High Altitude Aircraft Measured Radiance of White Sands, New Mexico, in the 450-1050 nm Band. Gilbert R. Smith, Robert H. Levin and John S. Knoll, April 1985. (PB85 204501/AS)

NESDIS 21 High Altitude Measured Radiance of White Sands, New Mexico, in the 400-2000nm Band Using a Filter Wedge Spectrometer. Gilbert R. Smith and Robert H. Levin, April 1985. (PB85 206084/AS)

NESDIS 22 The Space Station Polar Platform: NOAA Systems Considerations and Requirements. John H. McElroy and Stanley R. Schneider, June 1985. (PB86 6109246/AS)

NESDIS 23 The Use of TOMS Data in Evaluating and Improving the Total Ozone from TOVS Measurements. James H. Lienesch and Prabhat K. K. Pandey, July 1985. (PB86 108412/AS)

NESDIS 24 Satellite-Derived Moisture Profiles. Andrew Timchalk, April 1986. (PB86 232923/AS)

NESDIS 26 Monthly and Seasonal Mean Outgoing Longwave Radiation and Anomalies. Aronold Gruber, Marylin Varnadore, Phillip A. Arkin and Jay S. Winston, October 1987. (PB87 160545/AS)

NESDIS 27 Estimation of Broadband Planetary Albedo from Opertional Narrowband Satellite Measurements. James Wydick, April 1987. (PB88 107644/AS)

NESDIS 28 The AVHRR/HIRS Operational Method for Satellite Based Sea Surface Temperature Determination. Charles Walton, March 1987. (PB88 107594/AS)

NESDIS 29 The Complementary Roles of Microwave and Infrared Instruments in Atmospheric Soundings. Larry McMillin, February 1987. (PB87 184917/AS)

NESDIS 30 Planning for Future Generational Sensors and Other Priorities. James C. Fischer, June 1987. (PB87 220802/AS)

NESDIS 31 Data Processing Alogorithms for Inferring Stratospheric Gas Concentrations from Balloon-Based Solar Occultation Data. I-Lok Chang (American University) and Michael P. Weinreb, April 1987. (PB87 196424)

NESDIS 32 Precipitation Detection with Satellite Microwave Data. Yang Chenggang and Andrew Timchalk, June 1988. (PB88 240239)

NESDIS 33 An Introduction to the GOES I-M Imager and Sounder Instruments and the GVAR Retransmission Format. Raymond J. Komajda (Mitre Corp) and Keith McKenzie, October 1987. (PB88 132709)

NESDIS 34 Balloon-Based Infrared Solar Occultation Measurements of Stratospheric 03, H20, HNo3, and CF2C12. Michael P. Weinreb and I-Lok Chang (American University), September 1987. (PB88 132725)

NESDIS 35 Passive Microwave Observing From Environmental Satellites, A Status Report Based on NOAA's June 1-4, 1987, Conference in Williamsburg, VA. James C. Fisher, November 1987. (PB88 208236)

NESDIS 36 Pre-Launch Calibration of Channels 1 and 2 of the Advanced Very High Resolution Radiometer. C. R. Nagaraja Rao, October 1987. (PB88 157169/AS)

NESDIS 39 General Determination of Earth Surface Type and Cloud Amount Using Multispectral AVHRR Data. Irwin Ruff and Arnold Gruber, February 1988. (PB88 199195/AS)

NESDIS 40 The GOES I-M System Functional Description. Carolyn Bradley (Mitre Corp), November 1988.

NESDIS 41 Report of the Earth Radiation Budget Requirements Review - 1987, Rosslyn, VA, 30 March-3 April 1987. Larry L. Stowe (Editor), June 1988.

NOAA Technical Report NESDIS 75

DETECTION AND ANALYSIS OF FOG AT NIGHT USING GOES MULTISPECTRAL INFRARED IMAGERY

Gary P. Ellrod
Office of Research and Applications
Satellite Applications Laboratory
Physical Science Branch

Washington, D.C.
January 1994

U.S. DEPARTMENT OF COMMERCE
Ronald H. Brown, Secretary

National Oceanic and Atmospheric Administration
D. James Baker, Under Secretary

National Environmental Satellite, Data, and Information Service
Robert S. Winokur, Assistant Administrator

DETECTION AND ANALYSIS OF FOG AT NIGHT USING GOES MULTISPECTRAL INFRARED IMAGERY

Gary P. Ellrod
Satellite Applications Laboratory (NOAA/NESDIS)
Washington, DC

1. INTRODUCTION

The detection and short range forecasting of fog and low stratus clouds at night pose a difficult problem for aviation or marine meteorologists. The number of surface observing sites over land is insufficient to determine the true extent of fog, since many of these stations reduce operations at night. Weather reports from ocean going vessels are usually made at six hourly intervals and are concentrated on major shipping lanes. Because of the low density of these surface observations, especially at night, remote sensing techniques must be used to determine the coverage of fog and low clouds.

When fog is observed at an airfield, it is important to know its horizontal extent in order to estimate the time when it will dissipate. Using daylight visible imagery, Gurka (1978) observed that fog ususally dissipates from the outer edges inward. Clearing will thus occur sooner if the station is close to the upwind edge of the fog bank. Information on fog thickness is another important parameter that can be used to estimate dissipation time. The thicker the fog is, the longer the time required for clearing. Thus, knowledge of the location, movement and thickness of fog and stratus clouds during the predawn hours is critical for short range forecasts.

Infrared (IR) imagery from weather satellites such as the Geostationary Operational Environmental Satellite (GOES) operated by the United States is the primary tool for fog detection at night due to its relatively high frequency (30 min). The spatial resolution of the IR window channel, although limited to 8 km, is sufficient for fog detection. The greatest difficulty in the use of a single IR window channel is that the thermal contrast between fog and surrounding clear regions is often insufficient for proper detection, even with the use of image enhancement and animation techniques.

This paper describes a technique that uses two GOES IR window channels at different wavelengths to identify regions of fog or stratiform clouds at night regardless of existing surface temperatures. A method of estimating cloud thickness from this data will also be described. Examples of the effectiveness of this technique will be shown for cases of fog over: (1) flat terrain, (2) large bodies of water, and (3) mountainous, snow-covered regions.

2. BACKGROUND

Differences in the radiative properties of clouds observed in various visible and IR wavelengths were determined theoretically by Hunt (1973). It was found that clouds observed in the shorter wavelength (3.8μm) IR window (hereafter referred to as SIR) had a significantly lower emissivity[1] than at the longwave (11.0μm) IR (LIR) window for clouds containing either water droplets or ice particles. The variation of emissivity versus height above cloud base in the two IR channels and

---

[1]Emissivity is the ratio of emitted radiance to black body radiance, and is a measure of the transparency of an object to radiation from below. A thick cloud layer would have an emissivity close to 1.0.

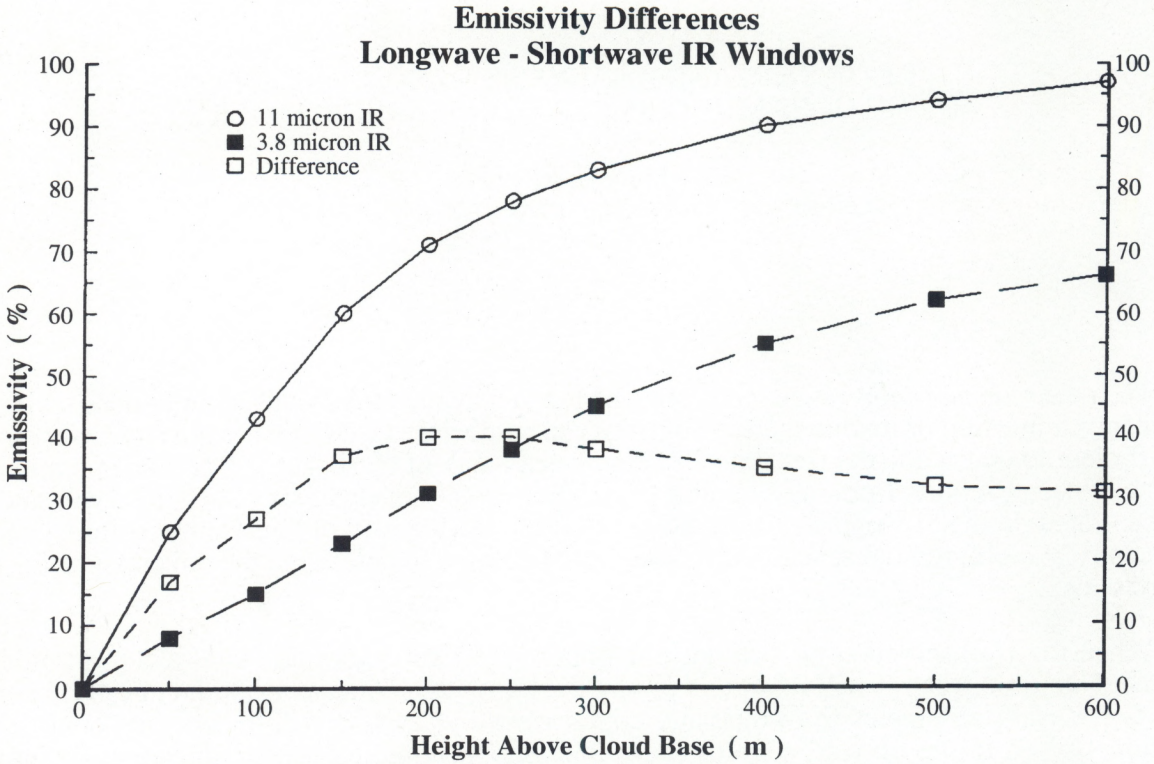

Figure 1. *The variation of emissivity (%) in a stratocumulus cloud of water content 0.1gm^{-3} for increasing height above cloud base (m). Emissivities are shown for Longwave (LW) IR channel (11μm), the Shortwave (SW) channel (3.8μm) and the difference between the two. (from Hunt, 1973)*

their differences for a stratocumulus cloud are shown in Figure 1.

The resulting temperature difference of a cloud observed by a satellite sensor in the two wavelengths is partly dependent on the atmospheric temperature profile below the cloud. Liquid stratiform clouds usually appear colder at night in the SIR channel than in the LIR channel because the clouds typically form within temperature inversions. Cooler radiance from within and below the clouds is more readily detected in the SIR channel, while the LIR channel senses primarily from near the cloud top. Conversely, ice phase cirrus clouds appear warmer in the SIR window since they are more thermally transparent in that wavelength range. In cloud-free regions, the temperature difference between the two channels is negligible. Although the temperature differences associated with fog and stratus are usually small (<<10°K), they are sufficient to provide clear discrimination of the cloud edge in most areas if the IR images are properly enhanced and displayed.

During daylight hours, there is a strong contribution from sunlight backscattered by liquid water clouds in the 3.5-4.0μm wavelengths. The reflected sunlight tends to negate the thermal differences of clouds in the window IR channels. As a result, the use of two window channels for fog detection is not effective during hours of sunlight. It is not needed then, however, since fog and stratus clouds have distinctive characteristics in high resolution (1 km) GOES visible imagery (i.e., Anderson, et al., 1974). One situation where the SIR imagery may be useful during daylight is in distinguishing low clouds from snow cover. The reflectance of sunlight off a snow covered surface in SIR is much smaller than that for liquid water clouds (Kidder and Wu, 1984). This difference results in improved brightness contrast between the clouds and snow cover. Sometimes this contrast is even better than in the LIR channel.

The first use of the bi-spectral technique in an operational forecast setting was accomplished in Great Britain (Eyre, et al., 1984). Imagery was used from the Advanced Very High Resolution Radiometer (AVHRR) onboard the NOAA (National Oceanic and Atmospheric Administration) polar-orbiting satellites. The AVHRR produces imagery in five spectral bands (4 IR, 1 Visible) with a spatial resolution of 1.1 km. The channels used for fog detection are: channel 3 centered near 3.7μm; and channel 4 at 11.0μm. Temperature differences ≥2.5°K were assumed to represent opaque cloud layers. For differences <0.5°K, clouds were assumed to be absent, and colors were assigned to discriminate land-water boundaries and other low level features. Intermediate temperature differences related to pixels (picture elements) that were partially filled with cloud or contained semi-transparent fog or cloud within a whole pixel.

In the United States, a similar approach was used with AVHRR data (d'Entremont and Thomason, 1987). They went one step further and combined information from channel 5 (12.0μm) to produce a color composite image that highlighted several different cloud types, including thin cirrus.

3. IMAGERY DERIVED FROM GOES DATA

The bi-spectral fog detection capability has more recently been demonstrated to be feasible using the lower resolution imagery from GOES (Ellrod, et al., 1989; Ellrod, 1991). Window IR data at 11.2μm wavelength is available in channel 8 (hereafter referred to as CH8). CH8 is produced every 30 minutes at a resolution of 8-10 km at midlatitudes. An equivalent to the AVHRR channel 3 is GOES channel 12 (3.9μm) (hereafter; CH12). CH12 has a resolution of only 15-17 km at midlatitudes, but it can still be used to derive imagery for detection of significant regions of fog or low clouds. The poor resolution will not permit observation of narrow valley fog in some cases.

The CH12 imagery is produced during the MultiSpectral Imaging (MSI) mode of operation that obtains IR data in 3 channels (normally including the 11μm window and 6.7μm water vapor). Prior to 1992, CH12 was only available several times per day, twice during the predawn hours. During late winter 1992, the frequency of CH12 IR data was increased to hourly to accomodate the "STORMFEST" research project in the central United States. The popularity and usefulness of the imagery was such that the hourly interval was retained after the project was ended. The higher frequency has permitted animation of the derived dual channel difference (hereafter referred to as DCD) imagery.

A version of the DCD imagery is in use at the National Aviation Weather Advisory Unit (NAWAU), a branch of the National Weather Service (NWS) in Kansas City, Missouri. The imagery is used to obtain information on the extent of low clouds for Area Forecasts (FAs) and short range advisories referred to as AIRMETs. Unfortunately, the DCD product is not yet distributed widely to users in the United States; it is only available at "National Centers" such as those in Washington, Miami and Kansas City.

4. IMAGE PROCESSING

The DCD imagery is routinely produced three times daily during the early morning hours at the NOAA Science Center in Camp Springs, Maryland. The images are processed at 0630, 0930 and 1130 UTC (corresponding to 0130, 0430 and 0630 Eastern Standard Time) on a Man-computer Interactive Data Analysis System (McIDAS) (Suomi, et al., 1983). After the raw digital image data are received, a program converts them to images of brightness temperature for both IR channels. In this format, large (small) brightness temperatures correspond to small (large) image brightness values. The CH12 image is then subtracted from the CH8 image. Positive values relate to

locations where CH12 is colder than CH8.

The brightness differences (in digital counts) are then modified for improved display according to the conversion shown in Table 1. Small changes in brightness become more easily observed because they are inflated, and placed in the middle range of the 0 to 255 count gray scale where the human eye is more sensitive. A difference of 2 digital counts in the GOES IR data is ≈1.0°K (Clark, 1983).

TABLE 1.
ASSIGNED OUTPUT IMAGE BRIGHTNESS

CH8 - CH12 Counts	OUTPUT BRIGHTNESS Counts
.	.
+2	136
+1	132
0	128
-1	124
-2	120
...etc	...etc

A smoothing program is then used to reduce the noise inherent to CH12 image data. The program determines the brightness value at any pixel by computing an average brightness for a 3 x 3 array centered on that pixel. A lookup table is then applied to the final image to further improve the contrast on the video display.

5. ESTIMATION OF FOG THICKNESS

After some experience with the DCD imagery, it was observed that the interior portions of extensive fog and stratus clouds seemed to be associated with larger DCD brightness difference (∂B) values. Fog depth is generally thought to be thicker in the interior part of the cloud, and thinner toward the edges. These observations suggested that quantitative estimates of fog depth could be extracted from the DCD imagery. This hypothesis is supported by calculations from Yamanouchi, et al., (1987), that showed an increase in the brightness temperature difference between NOAA AVHRR CHs 3 and 4 as the thickness of water clouds increase.

A sample of 80 cases was then collected in which the thickness of the fog layer was determined, along with the average ∂B value at the same location. A plot of the results along with a linear regression line of best fit is shown in Figure 2. A good relationship is observed with a correlation coefficient of 0.78. The dashed line in Figure 2 is an approximation of the data from Yamanouchi (1987) calculated for water clouds with a median drop diameter of 8μm (representative of fog) and a cloud temperature of 240°K. There is excellent agreement between the two lines.

In the observed GOES data sample shown in Figure 2, the fog thickness was estimated from the difference of the cloud top heights obtained from aircraft pilot reports (PIREPs) and the height of a nearby surface observing station in feet above mean sea level (MSL). The base of the cloud was assumed to be at the ground, since visibilities were required to be 0.5 miles (0.8 km) or less to be included in the sample. Since most aircraft reports are received after sunrise, there is usually a

time lag of at least 2-3 hours between the satellite image and the PIREPs. As a result, the fog thickness values obtained from Figure 2 are probably biased toward worst case values, since fog normally is thickest around sunrise.

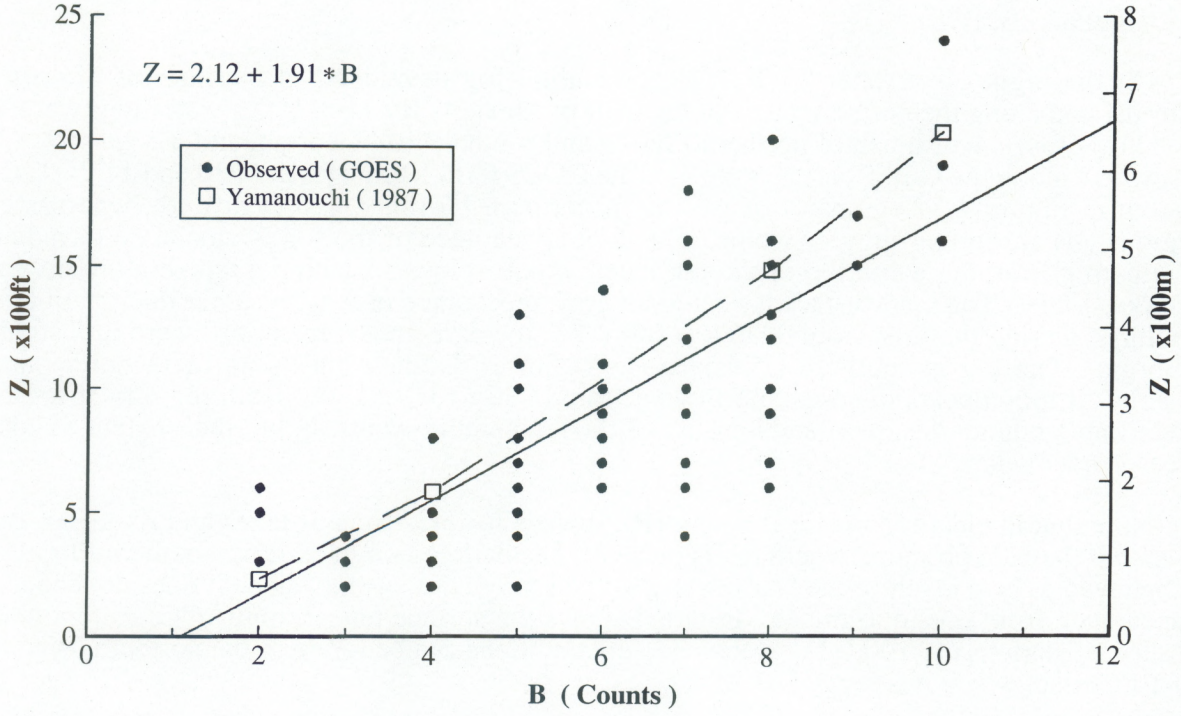

Figure 2. *Fog depth (ft and m) versus brightness differences (counts) between GOES IR CH12 (3.9μm) and CH8 (11μm). A least-squares regression line of best fit and its equation are shown. One count is ≈0.5° K. Data from Yamanouchi, et al., (1987) are shown for comparison.*

Both color and black-and-white enhancement tables were then developed to display the fog depth in intervals of 200 meters in a "step-wedge" pattern. The DCD imagery is normally smoothed over a 5x5 array so that the enhanced image can be easily interpreted. This smoothing tends to distort the original fog boundaries somewhat, and smaller, thinner fog patches are sometimes reduced or eliminated.

An independent data set of 27 cases was then collected to validate the enhancement technique. Fog thickness was determined in the same manner described above. The mean absolute error was about 70m (210 ft).

A technique to determine the time required for fog dissipation (in hours after sunrise) from enhanced GOES visible imagery was developed by Gurka (1978). The technique requires visible images at 1.5 hours after sunrise. The benefit of the IR technique described here is that it provides information needed for short range forecasts much earlier than the enhanced visible method. The conversion from fog depth to dissipation time can be made from other studies such as Wood (1938). A thickness of 600 m, for example, usually requires 4-6 hours to clear. This approach would obviously not work for advection type fogs in which the clouds are steadily replenished by the low level winds.

6. EXAMPLES

6.1 October 26, 1992

On the night of October 25-26, 1992, radiation fog developed in the interior of northern Florida, and along the northern coast of the Gulf of Mexico. By 1100 UTC, visibilities were 1 mi (1.6 km) or less over much of northern Florida and south central Georgia, and 3-5 mi (4.8-8 km) elsewhere along the Gulf Coast (Figure 3). The GOES CH8 IR images at 0930 and 1130 UTC are shown in Figure 4. Regions of dense fog in northern Florida (A) appear dark, whereas clear regions (B) are lighter gray or white. The dark appearance of the fog is attributed to radiation originating from the warm top of the fog layer, which is located within a temperature inversion (Gurka, 1980). The land surface has a lighter gray appearance in fog-free areas due to radiational cooling. During the time from 0930 to 1130 UTC, the dark area spread northward into southern Georgia. The fog in southern Louisiana (C) is not as distinct, but its northern border is still visible. It too appears to spread northward from 0930 to 1130 UTC. Both regions of fog have identifiable boundaries over land because of the temperature contrast, but their extent in coastal areas is not evident.

Note that in clear regions in Figure 4 (B), surface features such as lakes and rivers are easily seen, but they are obscured where fog is present. The dark region in extreme southern Florida (D) is believed to be a result of the warm water of the Everglades swamp, since it does not change its appearance from image to image. Figure 5 shows the surface temperatures (°C) as reported by observing stations at 1100 UTC. Much cooler conditions can be found in the northern clear areas (0-10°C) than where it is foggy (10-18°C).

GOES CH12 IR images at 0930 and 1130 UTC are shown in Figure 6. Due to the lower resolution of this channel, these images have a much grainier appearance than the CH8 images in Figure 4. The area of fog described above are also somewhat colder in CH12, as evidenced by the lighter gray shades in Figure 6. The cooler CH12 temperatures result in a loss of contrast between the fog and surrounding clear regions. In some warm season fog situations, CH12 can provide much better delineation of the boundary of the fog, but in this case, temperatures in the clear regions over land were too cool. However, the CH12 images do provide good depiction of the eastern edge of the fog off the east coast of Florida (E), and suggest that the fog in west central Florida (F) does not extend offshore.

A comparison of observed brightness temperatures for CHs 8 and 12 across the fog deck along G-G' (in Figure 4) is shown in Figure 7. CH12 (dotted line) is significantly cooler (2-4°K) than CH8 where dense fog was present, and slightly cooler (1-2°K) in the Florida panhandle where only minor visibility restrictions were observed. Note that the CH8 temperatures in the fog-free area of the Florida panhandle (282-283°K) are in good agreement with surface observations of 9°C (282°K) from Figure 5. In the Atlantic Ocean east of Florida, the temperature differences are negligible, although CH8 becomes slightly cooler than CH12. It is apparent that by obtaining the temperature difference between the two channels (a DCD image, defined earlier), discrimination of the fog will be less ambiguous, and less dependent on ambient surface temperature conditions.

The DCD images derived at 0930 and 1130 UTC are shown in Figure 8. The images are enhanced so that fog and stratus clouds are depicted as white to light gray. The areas of fog supported by surface observations over Florida, southeast Georgia, and Louisiana are clearly depicted. The slightly darker area in eastern Georgia and South Carolina shows the presence of shallow or non-opaque fog with visibilities from 2-6 miles. Darker shades of gray represent fog-free areas. Note that the dark region seen in Figure 4 over the Everglades Swamp in South

Florida appears dark in Figure 8, indicating clear conditions. The black patches in Louisiana, Arkansas and east Texas show a reversal in the CH 8-12 temperature relationship, suggesting the presence of cirrus clouds.

A smoothed image enhanced with a step wedge pattern to show approximate fog depth at 1130 UTC is shown in Figure 9. The outer dark gray shade represents depths of <200m, the light gray 200-400m and the black 400-600m. Aircraft PIREPs from 1324 to 1544 UTC indicated cloud tops at 300-360 m (1000-1200 ft) at Orlando (A) and Gainesville, Florida (B), decreasing to 150 m (500 ft) at Tampa (C) near the Gulf of Mexico. In southern Louisiana, the fog layer top was estimated by aircraft at 150 m (500 ft) at both Baton Rouge (D) and Lafayette (E). The PIREPs thus show good quantitative agreement with the satellite product.

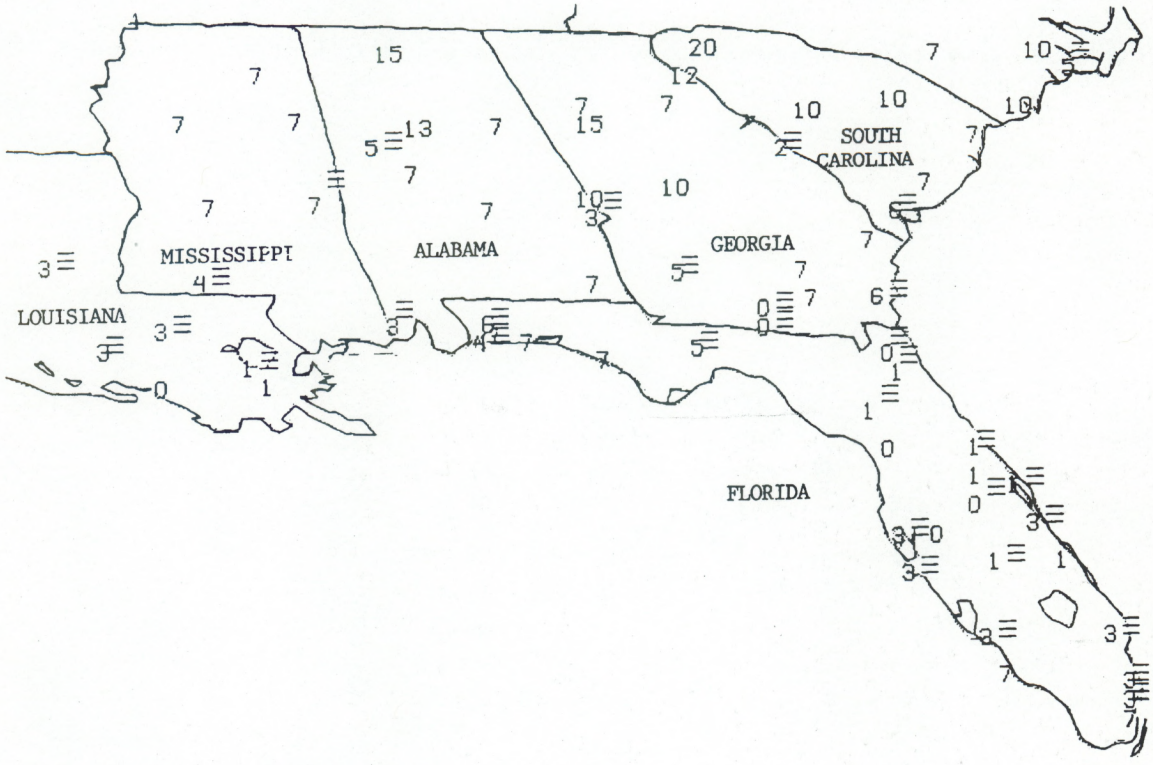

Figure 3. *Observed surface weather and visibility (mi) at 1100 UTC, 26 October 1992. The symbol ≡represents fog.*

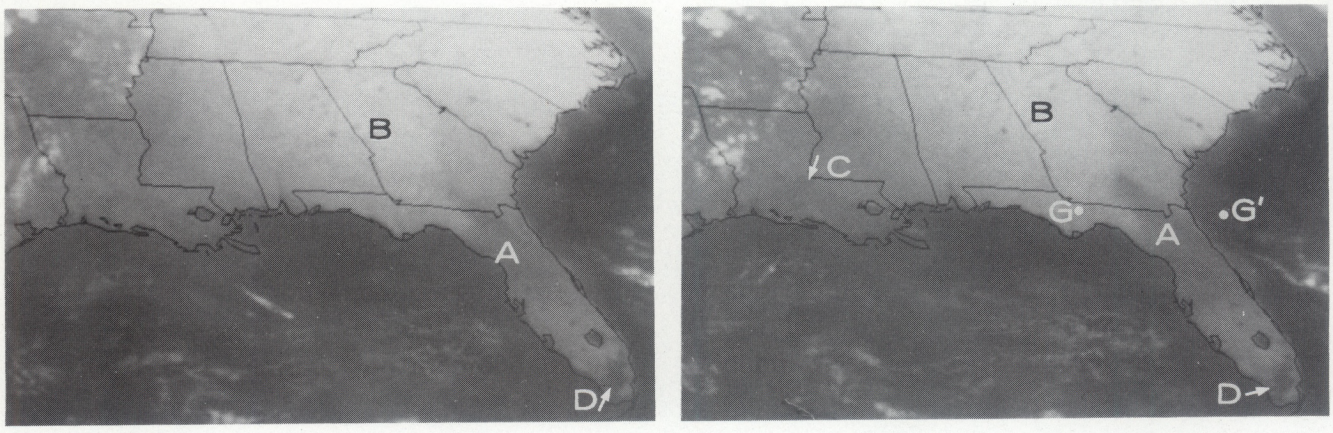

Figure 4. *GOES CH8 IR images at 0930 UTC (left) and 1130 UTC (right), 26 October, 1992.*

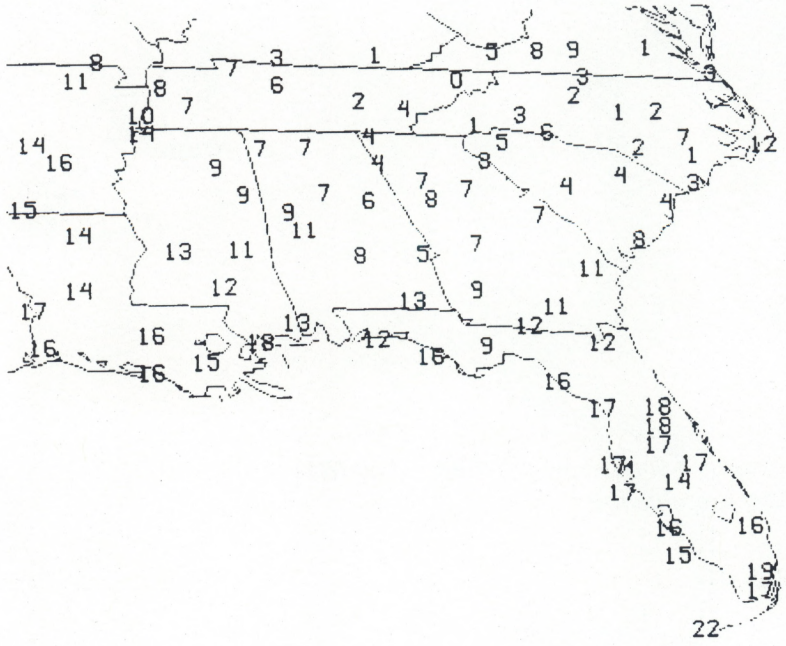

Figure 5. *Surface temperatures (°C) at 1100 UTC, 26 October 1992.*

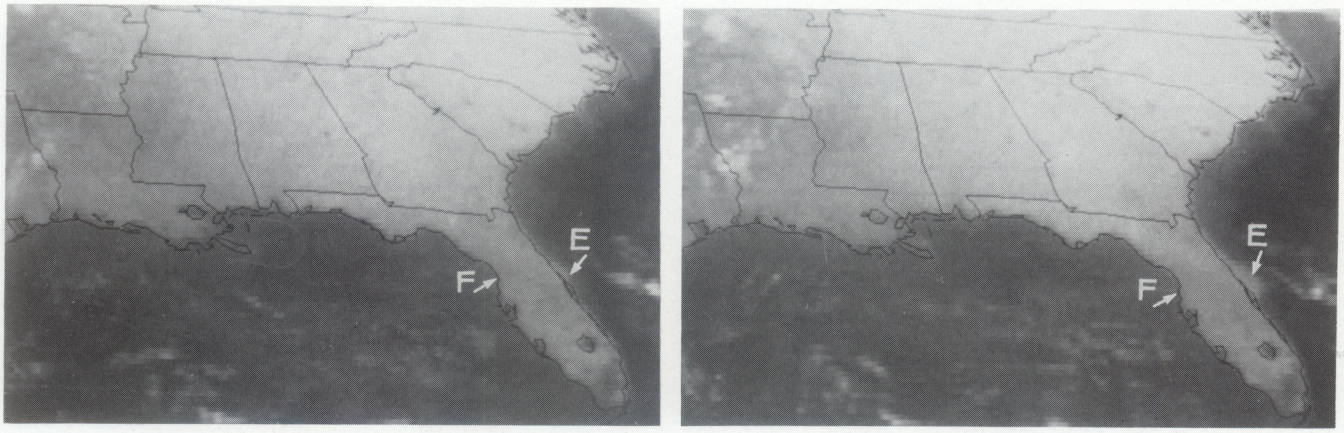

Figure 6. *Same as Figure 4, except for GOES CH12 (3.9μm).*

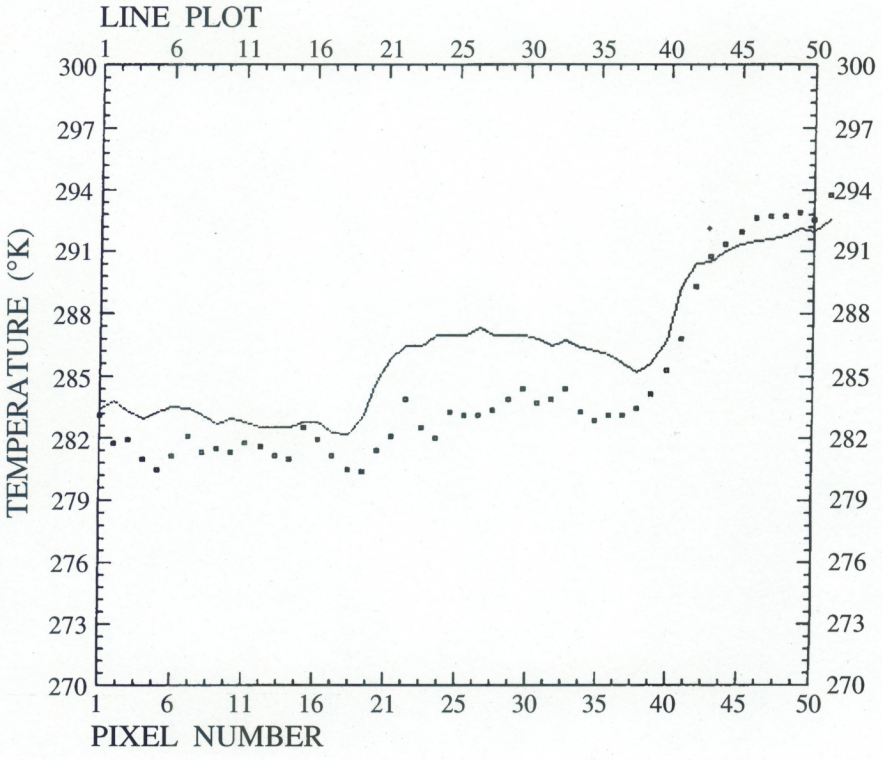

Figure 7. *A plot of brightness temperatures (°K) along the line G-G' in Figure 4. Solid line is from GOES CH8 (11.2μm), dashed line is from CH12 (3.9μm) IR.*

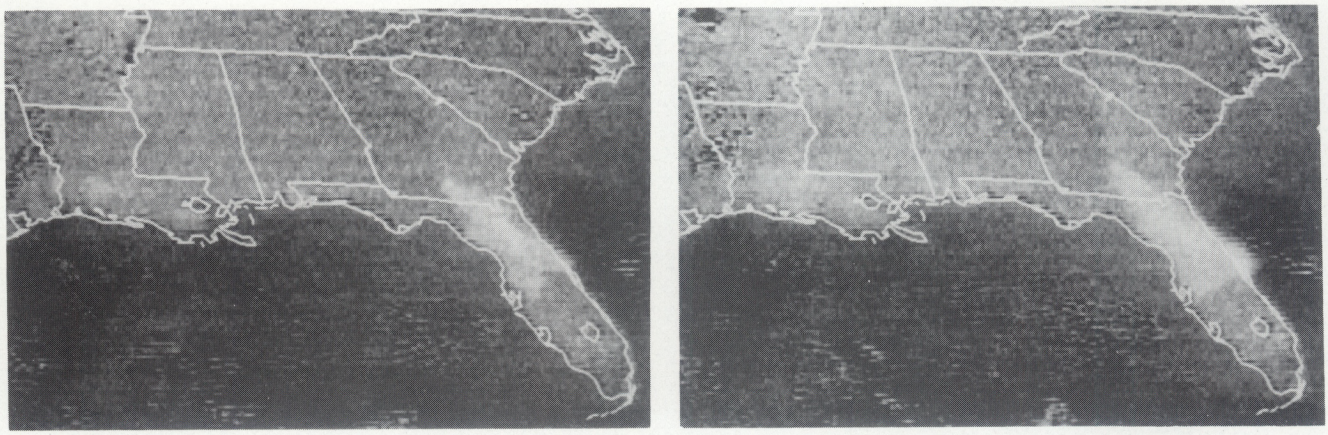

Figure 8. *Same as Figure 4, except GOES Dual Channel Difference (DCD) images based on subtraction of GOES CH12 from CH8 brightness temperatures.*

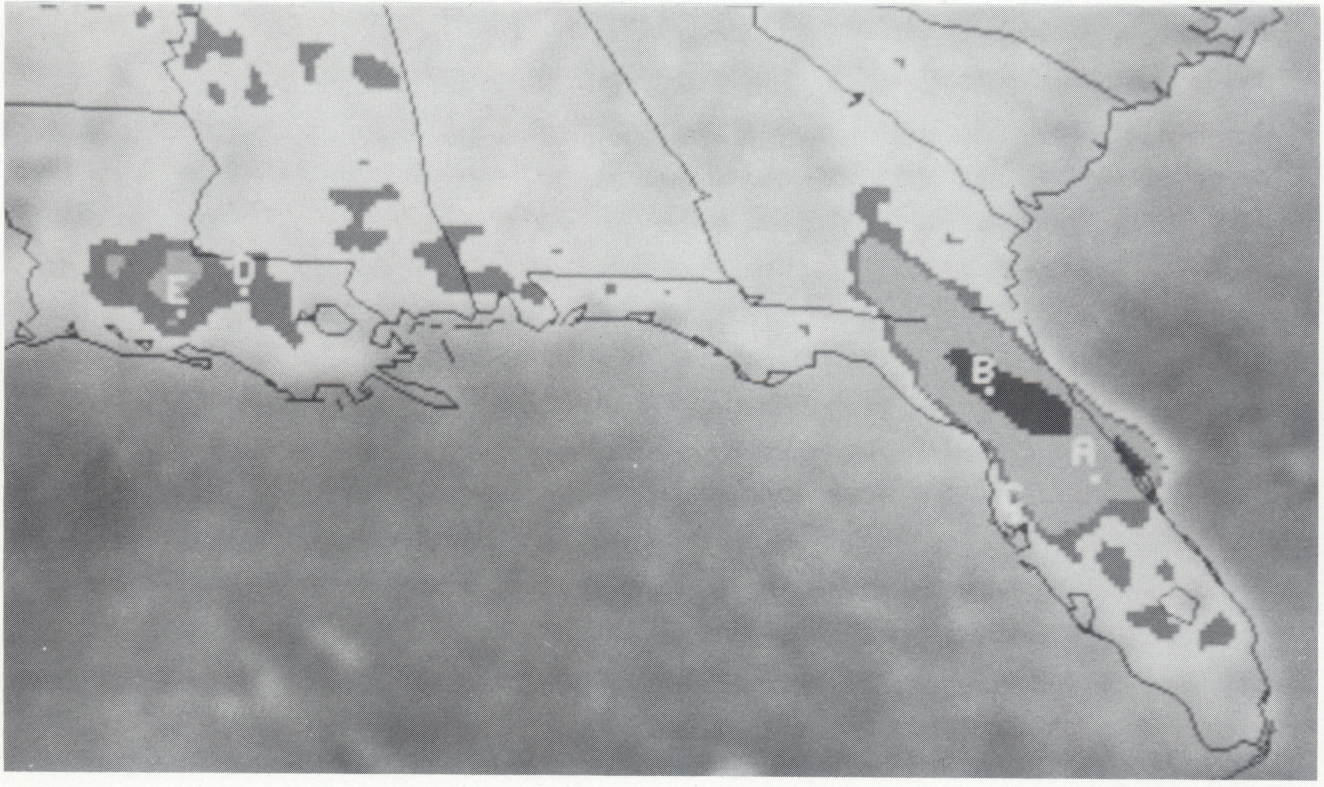

Figure 9. *Smoothed GOES DCD image enhanced to show approximate fog thickness in 200m intervals. Medium gray = <200m, light gray = 200-400m, black = 400-600m depth.*

6.2 February 4, 1991

During the early morning hours of February 4, 1991, extensive fog and low clouds were observed by surface stations along the coast of southern California in the Los Angeles Basin, and in the northern San Joaquin Valley (Figure 10). Visibility at 1000 UTC was near zero in some locales, and cloud ceilings were 220 m (700 ft) or less. Dense fog was also observed at several northern California inland locations.

The enhanced CH8 IR image at 0950 UTC (Figure 11) reveals a uniform light gray region offshore (3) associated with coastal stratus clouds. A dark patch could be seen in north central California (1) related to the dense valley fog. There was little evidence in this image for the coastal fog along the central coast (2).

The enhanced DCD image (Figure 12) clearly shows all three fog and stratus areas. The eastern boundary of the Los Angeles Basin fog is right along the coast, although it extends inland in a few places, notably near Los Angeles (LAX) and San Diego (SAN) (See Figure 10). The CH8 image suggests that the western boundary of the stratus is farther offshore than the DCD image shows, based on the extent of the gray area in Figure 11. The stratus is probably quite thin near its edge, so the DCD temperature differences are very small as a result.

The light gray patch near the mouth of the Colorado River (4) in the DCD image (Figure 12) is believed to be caused by thermal characteristics of the desert soil in that area. The patch is nearly always observed there, even though fog is rare at that location. Sutherland (1986) found that there are considerable differences in the calculated IR emissivity of soil types versus wavelength. At 3.75μm, for example, coarse sand had an emissivity of 0.793, while vegetated regions had and emissivity of 0.963. This difference could account for the bogus fog signature. Cirrus clouds which appear white in Figure 11, are black (5) in Figure 12.

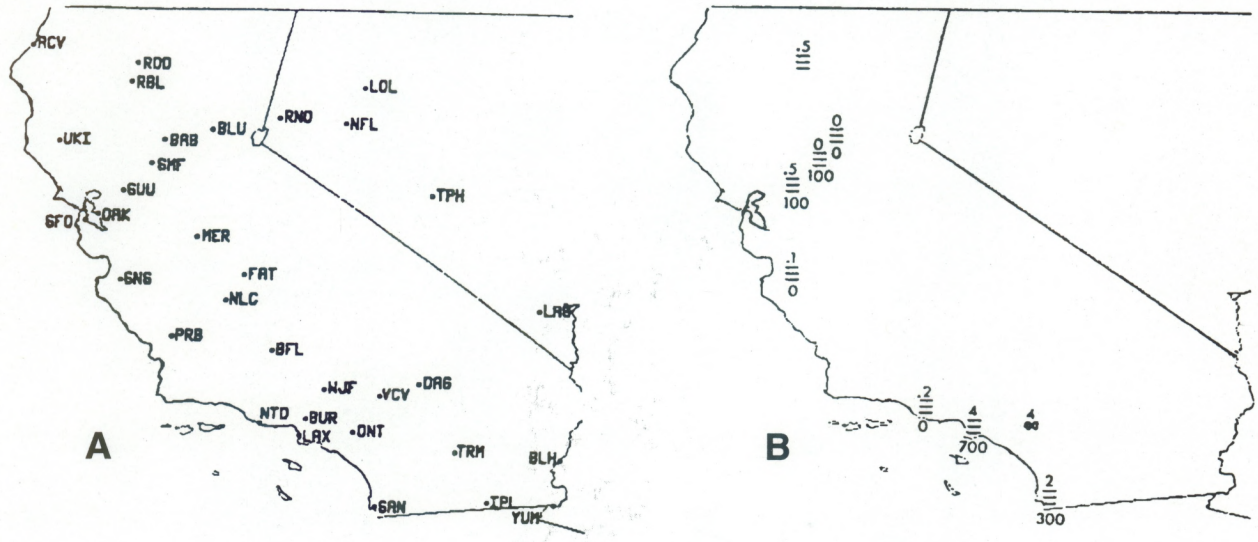

Figure 10. *(A) Surface weather reporting stations at 1000 UTC, February 4, 1991 and (B) Observed weather with cloud ceiling height in feet and visibility in miles. All other stations had ceilings > 6500 ft. (2km) and visibility > 7 miles (13km).*

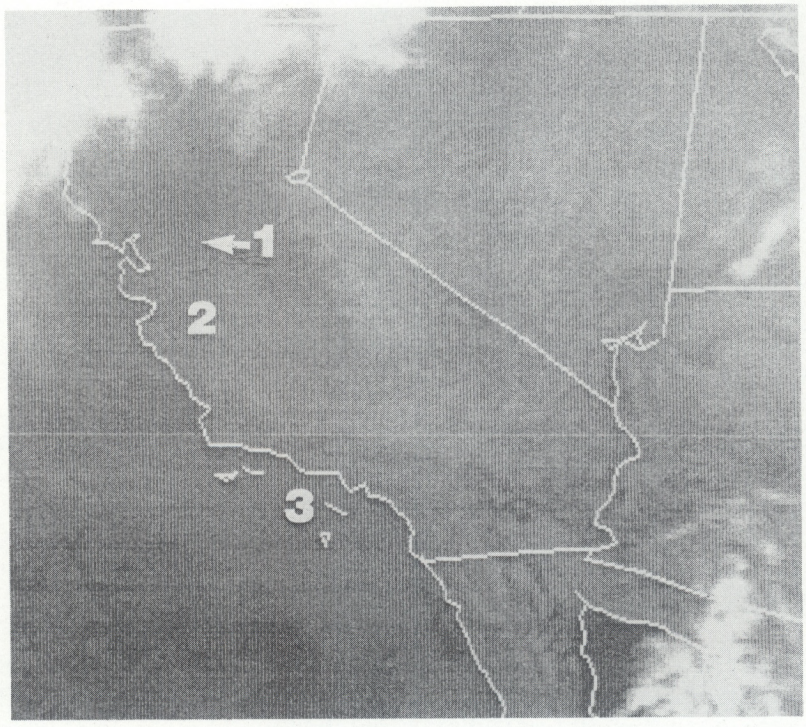

Figure 11. *Enhanced GOES CH8 IR image at 0950 UTC, February 4, 1991.*

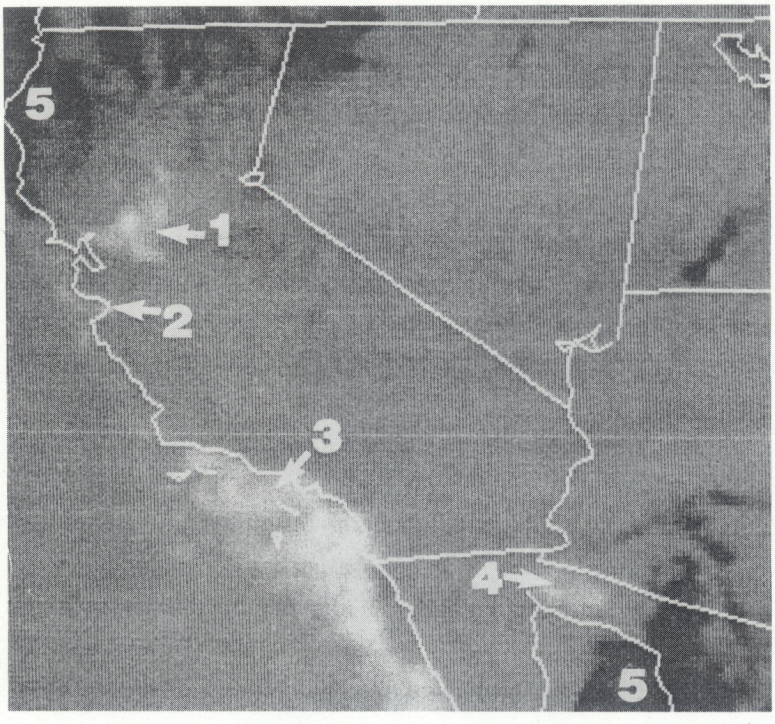

Figure 12. *GOES DCD image at 0950 UTC, February 4, 1991.*

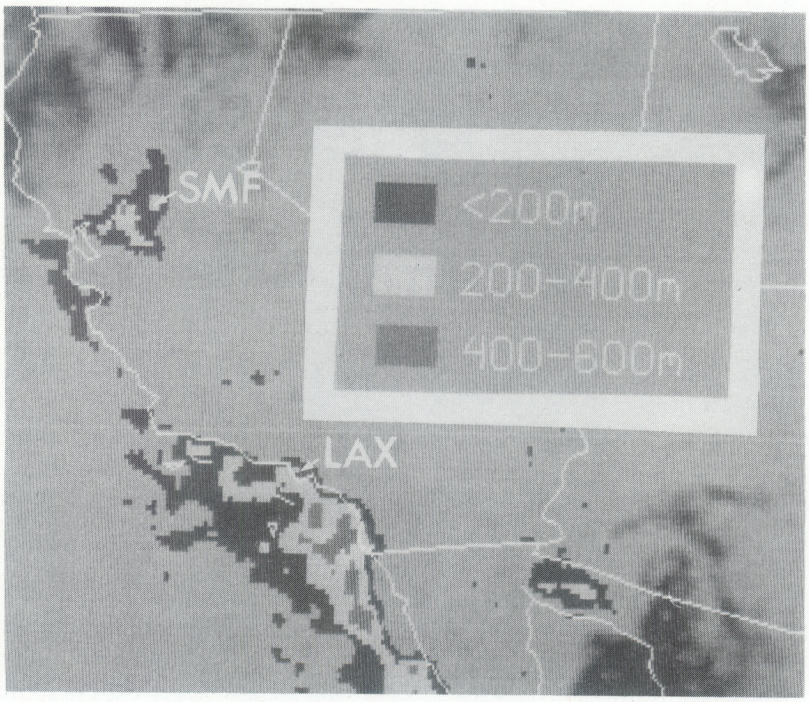

Figure 13. *Enhanced image that shows approximate fog depth at 0950 UTC, February 4, 1991.*

Enhanced imagery that contours approximate fog depth is shown in Figure 13. The imagery shows that most coastal and interior valley areas had fog/stratus depth in the 200-400 m range, with some denser areas just off the southern California coast. About 4 hours prior to this image time, an aircraft pilot reported fog tops at or below 400 m near Sacramento (SMF) in the northern valley. Reports around sunrise indicated that the stratus depth was a maximum of 500-600 m just south of LAX, but with 100-300 m prevalent farther inland. These aircraft reports confirmed that the satellite estimates were reasonable.

6.3 June 18, 1993

In the predawn hours on June 18, 1993, dense sea fog was present along the northeastern U. S. coast from New Jersey to Long Island. This fog extended well offshore, based on one ship observation, but the areal extent could not be determined without satellite imagery. Sea fog forms in this region in summer via the Taylor process in which warm moist air is cooled from below to its dew point temperature by waters of the southward-flowing Labrador Current.

Figure 14 shows an enhanced GOES CH8 IR image at 0630 UTC, superimposed by visibility (nm) from land and ship reports at 0600 UTC. The image has been remapped to a Mercator projection to correct for perspective problems near the horizon of the GOES viewing area. There was a report of near zero visibility about 100 nm east of Cape May, New Jersey. The IR image showed a bright white band of cirrus clouds (A) oriented northwest to southeast. To the east of the cirrus (B), the ocean surface is observed to be slightly darker (warmer) over a large region east of New Jersey than farther to the northeast (C) (southeast of Cape Cod), where visibility is reported

to be unrestricted. While fog is suspected in area B, the boundary of the fog deck is difficult to discern from the CH8 IR satellite image.

The GOES CH12 image (Figure 15) at 0630 UTC shows most of the suspected foggy area to be a slightly lighter gray shade than in CH8, indicating cooler temperatures. This information still does not provide unambiguous delineation of the fog area.

The DCD image at this time, however, (Figure 16) shows that fog is present over most of the offshore waters west of 70° W and north of 38° N. A couple of large open areas are present near the coast of Long Island (D). The latter could be seen in CH12 (Figure 15), but not in CH8 (Figure 14).

The sea fog was estimated to be <200m in depth near the coast and 200-400m thick well offshore based on the satellite enhancement of the DCD product (Figure 17). An aircraft report from southwest Cape Cod 4 hours later indicated that the fog was about 400 ft (160m) thick.

Direct confirmation of the cloud coverage could not be obtained until six hours later when visible imagery became available. The GOES visible image at 1230 UTC (Figure 18) superimposed with visibility reports indicates that the DCD image was probably representative of the actual fog coverage at 0630 UTC. The fog had spread northeastward along the coast in the 6 hour period because of the prevailing southwesterly flow and the development of new sea fog. A large open area is present along the eastern end of Long Island that could be one of the two shown in Figure 15-16. Figure 19 shows surface winds for this region at 1200 UTC that were from the southwest at 10 to 15 knots in the offshore waters.

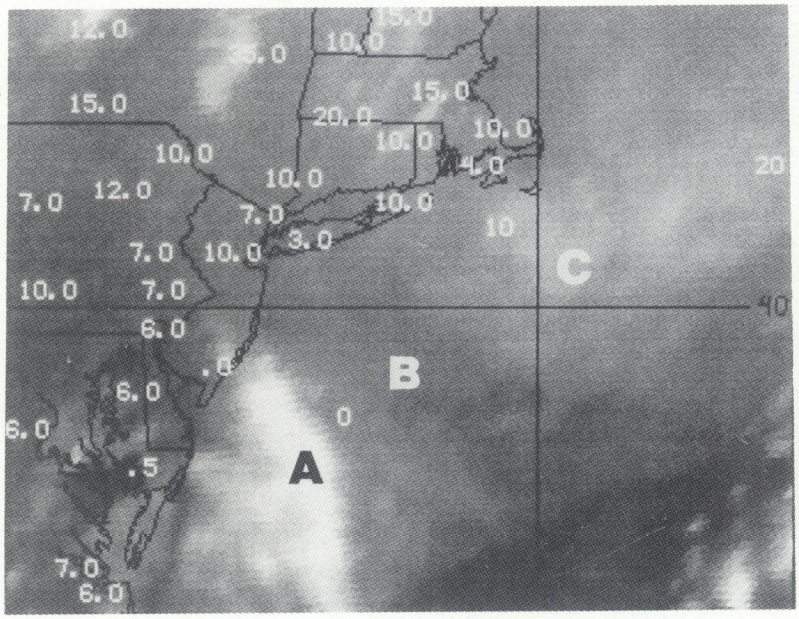

Figure 14. *Enhanced GOES CH8 IR at 0630 UTC, June 18, 1993. The image is remapped into a Mercator projection. Visibilities (nm) are superimposed.*

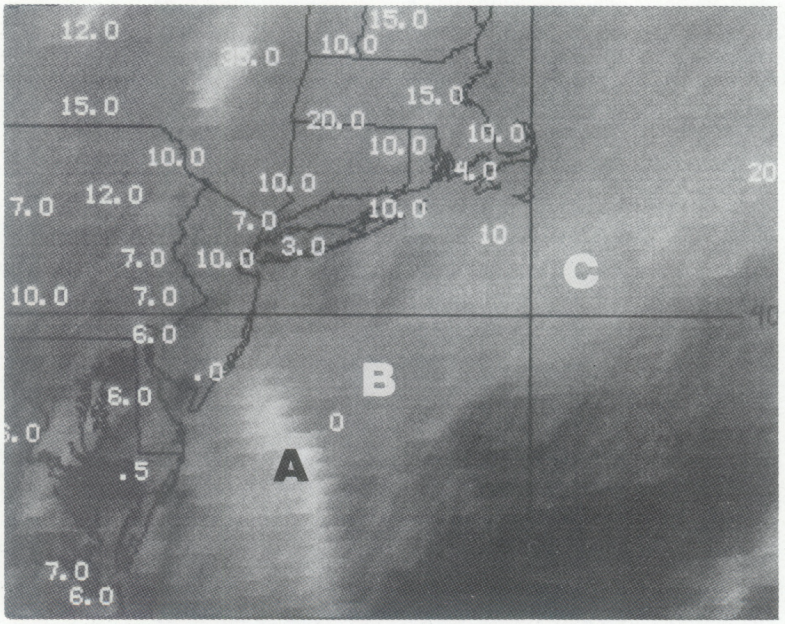

Figure 15. *Enhanced GOES CH12 IR image at 0630 UTC, June 18, 1993.*

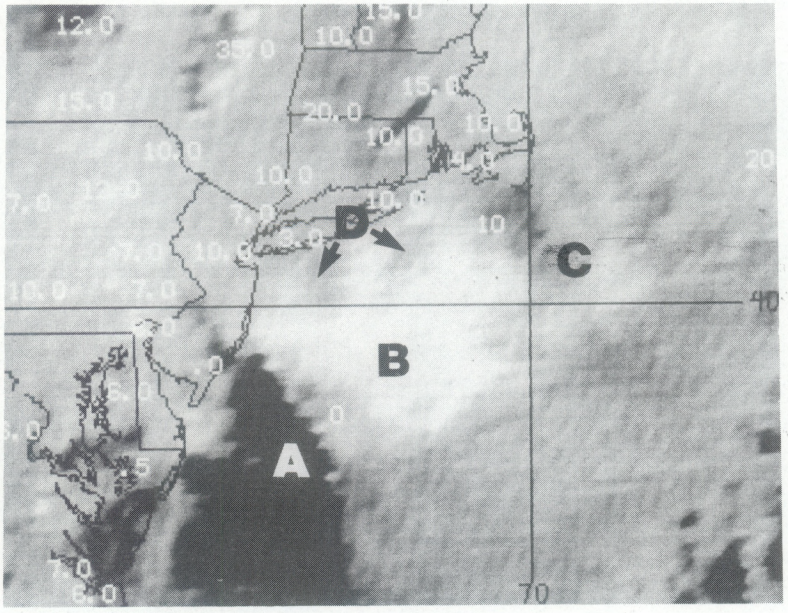

Figure 16. *Enhanced GOES DCD image at 0630 UTC, June 18, 1993.*

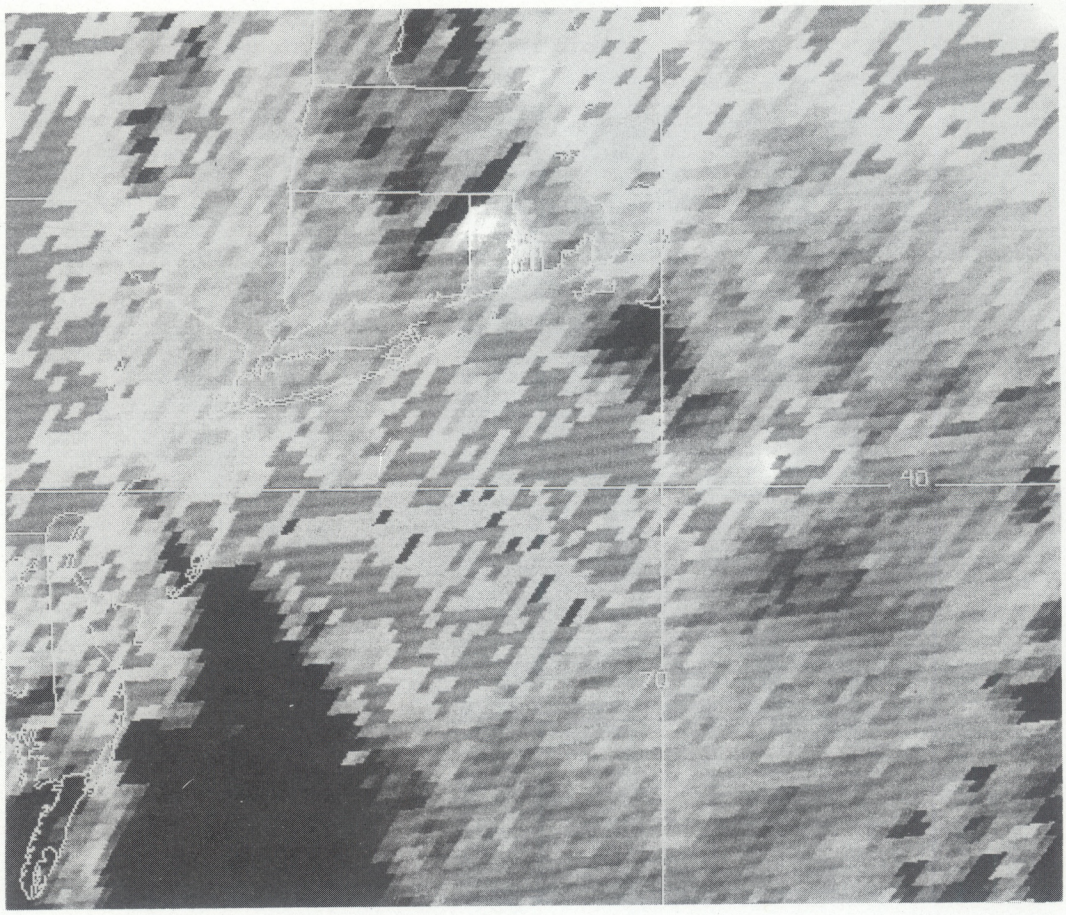

Figure 17. *Approximate fog depth at 0630 UTC, June 18, 1993. The gray scale enhancement is the same as in Figure 9.*

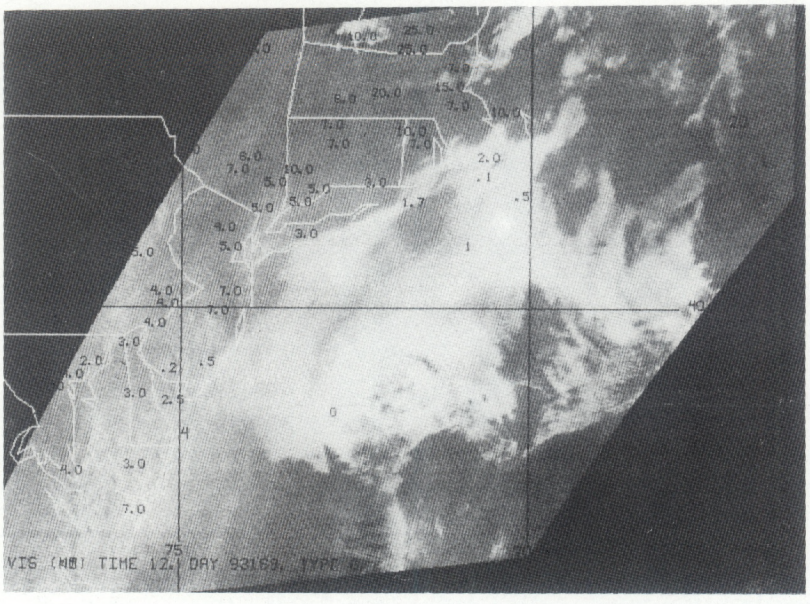

Figure 18. *GOES visible image at 1230 UTC, June 18, 1993.*

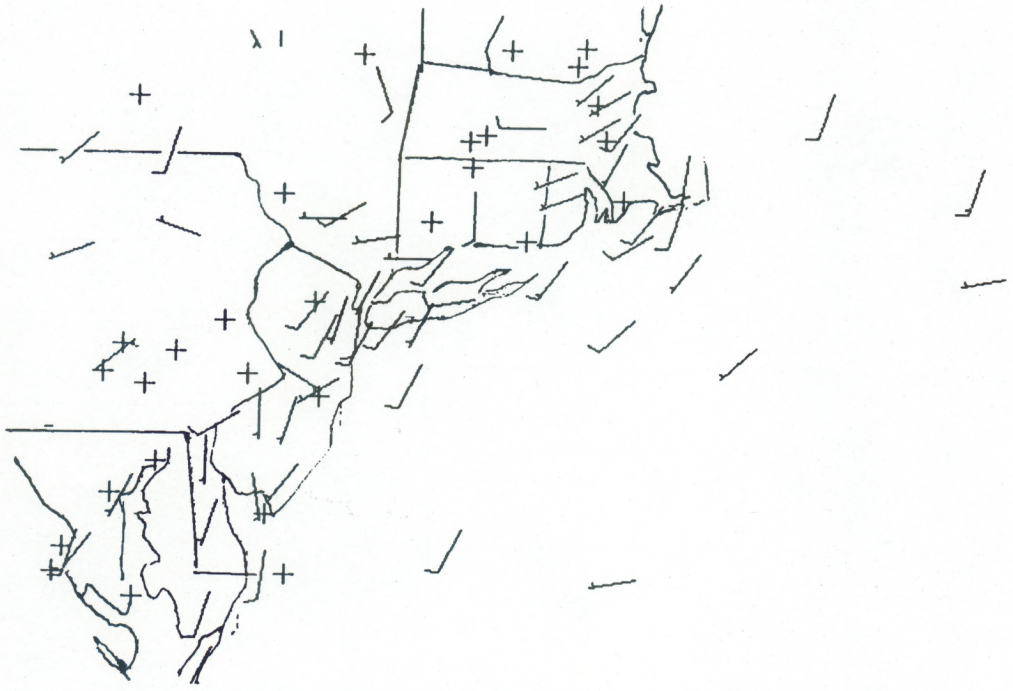

Figure 19. *Surface winds at 1200 UTC, June 18, 1993.*

6.4 February 4, 1993

An area of stagnant high pressure covered the Great Basin and Pacific Northwest states on the morning of February 4, 1993, resulting in light winds and radiational cooling. Visibilities at 1300 UTC (Figure 20) were reduced in fog and low clouds over parts of Oregon, Idaho, Utah, Wyoming, and Colorado.

The GOES enhanced CH8 IR image (Figure 21) shows what is at first glance a bewildering assortment of gray patterns caused by a combination of various cloud types and terrain features. Surface temperatures (Figure 22) were -15 to -25°C (+5 to -13°F) from eastern Idaho southeastward across Colorado, and 0 to -15°C (32 to 5°F) elsewhere. Much of the northern Rockies area was snow-covered (Figure 23), enhancing the radiational cooling where clouds were absent. From southern Montana southward to Colorado and northeast Utah, terrain features such as dendritic river valleys were evident in Figure 21, indicating clear conditions. Bright filaments of cold clouds across western Montana, Idaho, and Utah suggested the presence of cirrus. Medium grey shades and uniform texture over southeast Oregon, northern Nevada and southwest Idaho support the presence of altostratus clouds. Low clouds were very difficult to distinguish in any areas, however.

The CH12 image alone (Figure 24) did not provide any more information except that some of the cloudy areas appeared somewhat whiter (colder). As temperatures become colder, the instrument noise in CH12 increases, which is apparent in this example, especially in clear regions of the northern Rockies.

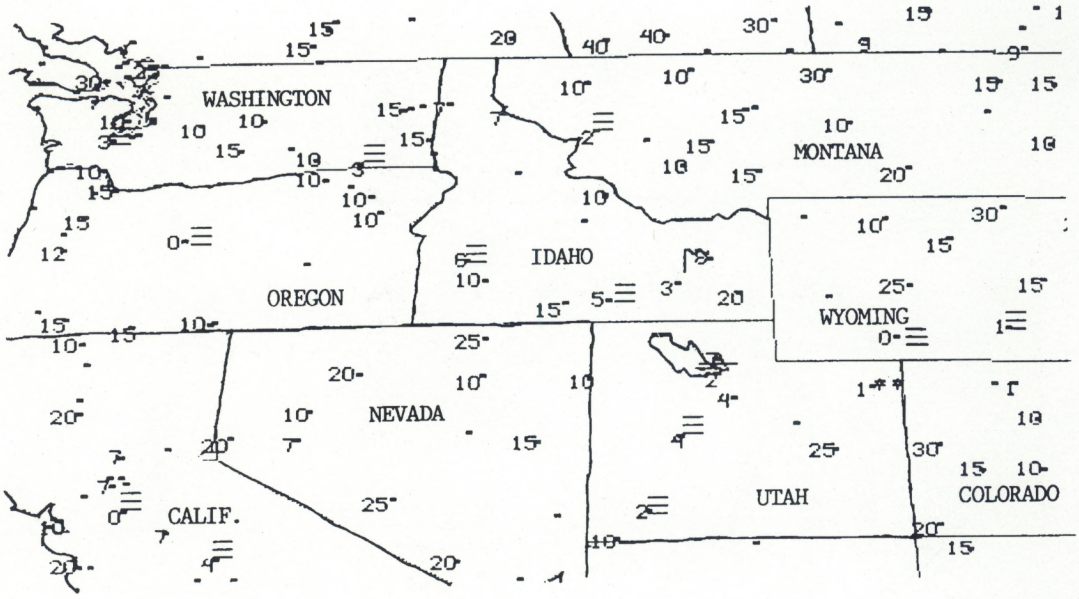

Figure 20. *Observed surface weather and visibility (mi) at 1300 UTC, February 4, 1993.*

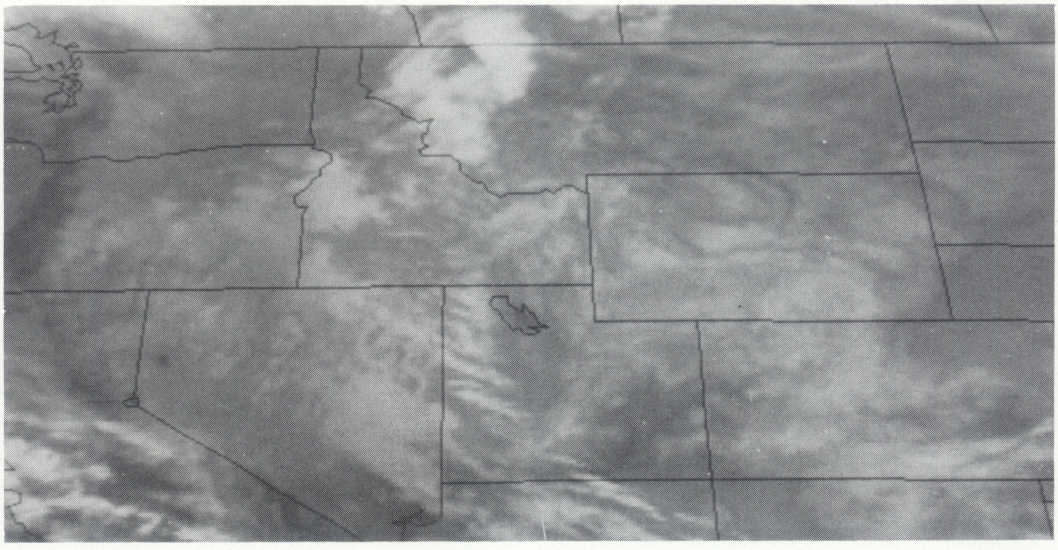

Figure 21. *Enhanced GOES CH8 IR image at 1330 UTC, February 4, 1993.*

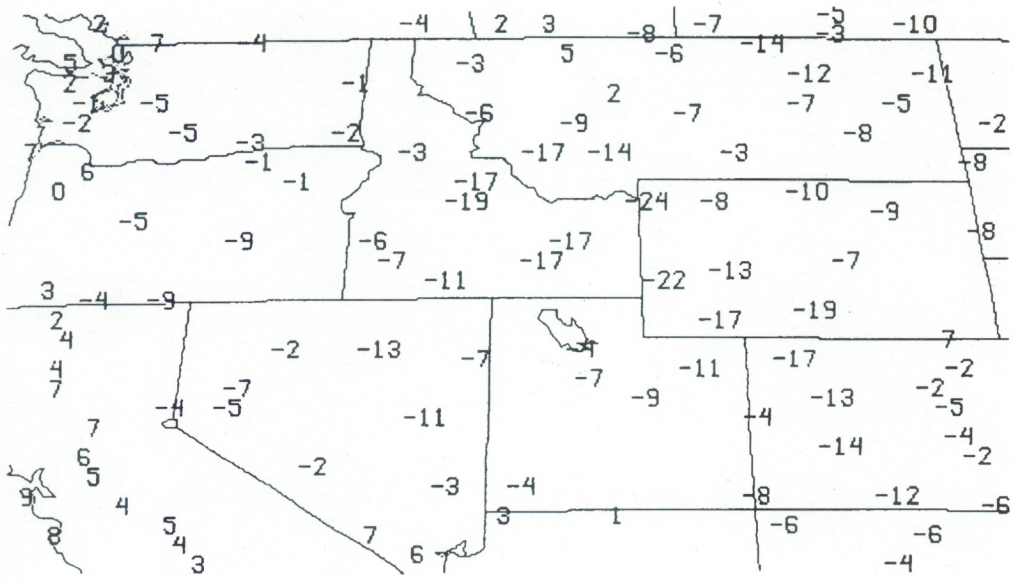

Figure 22. *Surface temperatures (°C) at 1300 UTC, February 4, 1993.*

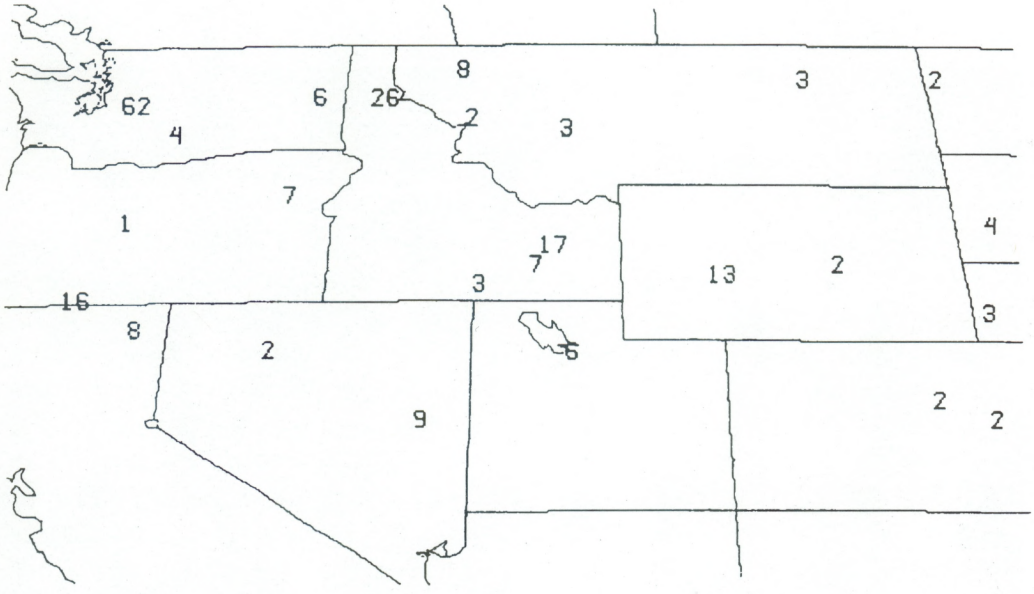

Figure 23. *Snow depth (in) observed at 1200 UTC, February 4, 1993.*

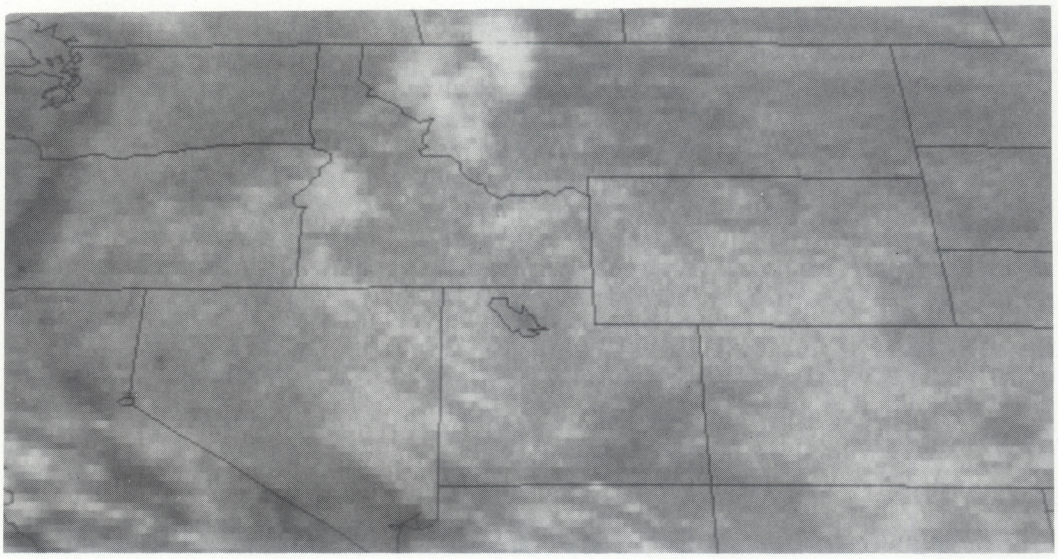

Figure 24. *Enhanced GOES CH12 IR image at 1330 UTC, February 4, 1993.*

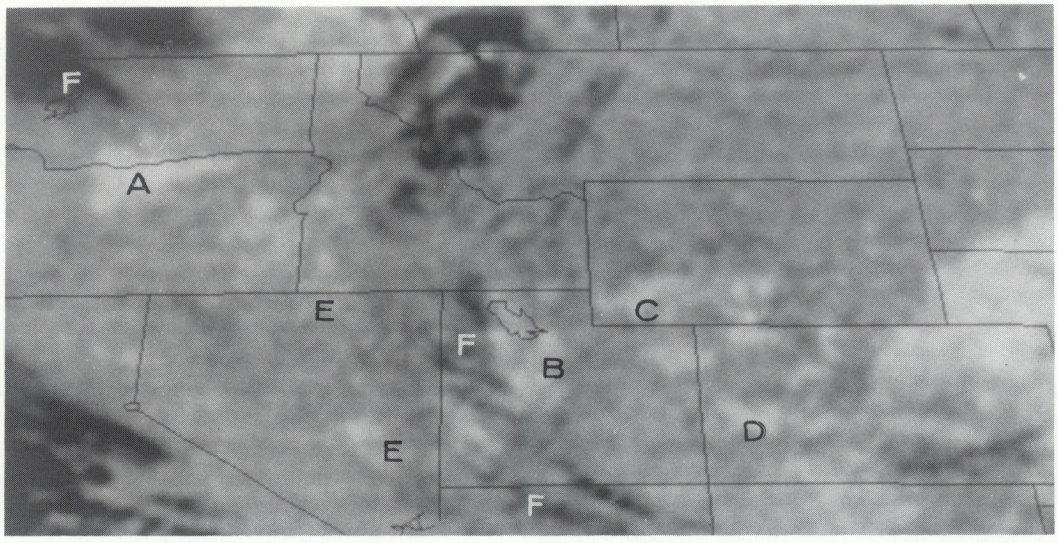

Figure 25. *GOES DCD image at 1330 UTC, February 4, 1993.*

The smoothed DCD image (Figure 25) offers a better tool for locating cloudy or foggy regions, and provides information on cloud types. Areas of dense fog or stratus along the Columbia River and central Oregon (A), the Salt Lake Valley of Utah (B), southern Wyoming (C), and western Colorado (D) appear white. The middle level altostratus clouds previously described are a slightly darker, mottled gray tone (E). The clouds identified as cirrus from the CH8 IR image appear black in the DCD image (F).

The DCD image shows the horizontal extent of low clouds that was not evident from the CH8 IR window image alone. Where even thin cirrus is present, however, the low cloud signal in the DCD image is contaminated, and the lower clouds are not detectable. This effect is present over parts of western Montana, southern Idaho, and Utah.

The fog depth enhancement of the DCD image (not shown) indicated that the fog and stratus was 200-400m thick. No direct verification could be obtained, however.

7. SUMMARY AND CONCLUSIONS

A technique that detects the presence of fog or low stratiform clouds at night from the digital subtraction of brightness temperatures for two GOES IR window channels (at 11.2 and 3.9μm wavelengths) has been described. The resulting Dual Channel Difference (DCD) imagery is effective over a wide range of terrain and temperature regimes. It has also been shown to be useful over both snow-covered surfaces and oceans.

A step-wedge enhancement technique for quantitative estimates of fog thickness is accurate to within 100m, provided that thin high cloud layers are not present. The depth estimates can then be used by aviation forecasters to help determine the approximate dissipation time of the fog. The instrument noise inherent in CH12 requires considerable smoothing to make the fog depth product useful, resulting in slight distortion of the contours.

There are some limitations to the effectiveness of the DCD imagery. The low resolution (15 km) of DCD imagery does not allow detection of narrow fingers of valley fog in some situations. There is also difficulty in resolving shallow fog layers because the small temperature differences present (1-2°C) are within the instrument noise of GOES CH12.

The advanced GOES-I satellite, to be launched in 1994, will have 3.9μm IR imagery with a resolution of 4 km, an improvement by better than a factor of three. The imagery will also be available at a minimum of every 30 minutes, compared to hourly with the current GOES satellite. Reduction in the instrument noise is also expected.

Multispectral IR image differencing techniques using the 3.9μm and 11.2μm channels from GOES show considerable promise in the detection of hazardous fog and low clouds for aviation and marine weather forecasting. The expected improvements in the GOES satellite instruments will encourage more widespread use of these derived products in the coming years.

8. ACKNOWLEDGEMENTS

The author would like to thank Frances Holt of NESDIS, Doug Mathews of NWS/NAWAU in Kansas City, Jim Gurka of the NWS Boston, and George Bancroft and Dave Feit of the NMC Marine Forecast Branch in Washington for their review of this report. Lori Paschal edited and formatted the text. Phil Golden of Planning Research Corporation processed the photographs. Paige Bridges completed the final layout.

9. REFERENCES

Anderson, R.K., et al., 1974: Application of meteorological satellite data in analysis and forecasting. ESSA Tech. Report NESC 51, U. S. Dept. of Commerce, Washington, DC, page 6-B-1.

Clark, J. D. (Ed.), 1983: The GOES User's Guide. U. S. Dept. of Commerce, National Oceanic and Atmospheric Administration (NOAA), Washington, DC.

D'entremont, R. P. and L. W. Thomason, 1987: Interpreting meteorological satellite images using a color-composite technique. Bull. Amer. Meteor. Soc., 68, 762-768.

Ellrod, G. P., 1991: Nighttime fog detection with bi-spectral GOES-VAS imagery. Proceedings, Fourth International Conference on Aviation Weather Systems, May 24-28, 1991, Paris, France. Amer. Meteor. Soc., Boston, 71-75.

_____, E. Maturi, and Lt (jg) J. Steger, 1989: Detection of fog at night using dual channel GOES-VAS imagery. Proceedings, Twelfth Conference on Weather Analysis and Forecasting, October 2-6, 1989, Monterey, California, Amer. Meteor. Soc., Boston, 515-520.

Eyre, J. R., J. L. Brownscombe and R. J. Allam, 1984: Detection of fog at night using Advanced Resolution Radiometer (AVHRR) imagery. Meteorological Magazine, 113, 266-271.

Gurka, J. J., 1978: The role of inward mixing in the dissipation of fog and stratus. Mon. Wea. Rev., 106, 1633-1635.

Gurka, J. J., 1978: The use of enhanced visible imagery for predicting the time of fog dissipation. Proceedings, Conf. on Weather Forecasting and Analysis and Aviation Meteorology, October 16-19, 1978, Silver Spring, Maryland, Amer. Meteor. Soc., Boston, 343-346.

_____, 1980: Observations of advection-radiation fog formation from enhanced IR satellite imagery. Proceedings, Eighth Conf. on Weather Forecasting and Analysis, June 10-13, 1980, Denver, Colorado, Amer. Meteor. Soc., Boston, 108-114.

Hunt, G. E., 1973: Radiative properties of terrestrial clouds at visible and infrared thermal window wavelengths. Quart. J. Royal Meteor. Soc., 99, 346-369.

Kidder, S. Q., and H. -T. Wu, 1984: Dramatic contrast between low clouds and snow cover in daytime 3.7μm imagery. Mon. Wea. Rev., 112, 2345-2346.

Sutherland, R. S., 1986: Broadband and spectral emissivities (2-18 μm) of some natural soils and vegetation. J. Atmos. Oceanic Tech., 3, 199-202.

Suomi, V. E., R. Fox, S. S. Limaye, and W. L. Smith, 1983: McIDAS III: A modern interactive data access and analysis system. J. Cli. and Appl. Meteor., 22, 766-778.

Wood, F. B., 1938: The formation and dissipation of stratus clouds beneath turbulent inversions. Bull. Amer. Meteor. Soc., 19, 97-103.

Yamanouchi, T., K. Suzuki, and S. Kawaguchi, 1987: Detection of clouds in Antarctica from infrared multispectral data of AVHRR. J. Meteor. Soc. of Japan, 65, 949-96

(Cont'd from front inside cover)

NESDIS 42 Simulation Studies of Improved Sounding Systems. H. Yates, D. Wark, H. Aumann, N. Evans, N. Phillips, J. Sussking, L. McMillin, A. Goldman, M. Chahine and L. Crone, February 1989.

NESDIS 43 Adjustment of Microwave Spectral Radiances of the Earth to a Fixed Angle of Progagation. D. Q. Wark, December 1988. (PB89 162556/AS)

NESDIS 44 Educator's Guide for Building and Operating Environmental Satellite Receiving Stations. R. Joe Summers, Chambersburg Senior High, February 1989.

NESDIS 45 Final Report on the Modulation and EMC Consideration for the HRPT Transmission System in the Post NOAA-M Polar Orbiting Satellite ERA. James C. Fisher (Editor), June 1989. (PB89 223812/AS)

NESDIS 46 MECCA Program Documentation. Kurt W. Hess, September 1989.

NESDIS 47 A General Method of Using Prior Information in a Simultaneous Equation System. Lawrence J. Crone, David S. Crosby and Larry M. McMillin, October 1989.

NESDIS 49 Implementation of Reflectance Models in Operatioal AVHRR Radiation Budget Processing. V. Ray Taylor, February 1990.

NESDIS 50 A Comparison of ERBE and AVHRR Longwave Flux Estimates. A. Gruber, R. Ellingson, P. Ardanuy, M. Weiss, S. K. Yang, (Contributor: S.N. Oh).

NESDIS 51 The Impact of NOAA Satellite Soundings on the Numerical Analysis and Forecast System of the People's Republic of China. A. Gruber and W. Zonghao, May 1990.

NESDIS 52 Baseline Upper Air Network (BUAN) Final Report. A. L. Reale, H. E. Fleming, D. Q. Wark, C. S. Novak, F. S. Zbar, J. R. Neilon, M. E. Gelman and H. J. Bloom, October 1990.

NESDIS 53 NOAA-9 Solar Backscatter Ultraviolet (SBUV/2) Instrument and Derived Ozone Data: A Status Report Based on a Review on January 29, 1990. Walter G. Planet, June 1990.

NESDIS 54 Evaluation of Data Reduction and Compositing of the NOAA Global Vegetation Index Product: A Case Study. K. P. Gallo and J. F. Brown, July 1990.

NESDIS 55 Report of the Workshop on Radiometric Calibration of Satellite Sensors of Reflected Solar Radiation, March 27-28, 1990, Camp Springs, MD. Peter Abel (Editor), July 1990.

NESDIS 56 A Noise Level Analysis of Special 10-Spin-Per-Channel VAS Data. Donald W. Hillger, James F. W. Purdom and Debra A. Lubich, February 1991.

NESDIS 57 Water Vapor Imagery Interpretation and Applictions to Weather Analyis and Forecasting. Roger B. Weldon and Susan J. Holmes, April 1991.

NESDIS 58 Evaluating the Design of Satellite Scanning Radiometers for Earth Radiation Budget Measurements with System, Simulations. Part 1: Instantaneous Estimates. Larry Stowe, Philip Ardanuy, Richard Hucek, Peter Abel and Herberet Jacobowitz, October 1991.

NESDIS 59 Interactive Digital Image Display and Analysis System (IDIDAS) User's Guide. Peter J. Celone and William Y. Tseng, October 1991.

NESDIS 60 International Dobson Data Workshop Summary Report. Robert D. Hudson (University of Maryland) and Walter G. Planet, February 1992.

NESDIS 61 Tropical Cyclogenesis in the Western North Pacific. Raymond M. Zehr, July 1992.

NESDIS 62 NOAA Workshop on Climate Scale Operational Precipitation and Water Vapor Products. Ralph Ferraro (Editor), October 1992.

NESDIS 63 A Systematic Satellite Approach for Estimating Central Pressures of Mid-Latitude Oceanic Storms. Frank J. Smigielski and H. Michael Mogil, December 1992.

NESDIS 64 Adjustment of TIROS Operational Vertical Sounder Data to a Vertical View. David Q. Wark, March 1993.

NESDIS 65 A Noise Level Analysis of Special Multiple-Spin VAS Data During Storm-fest. Donald W. Hillger, James F.W. Purdom and Debra A. Molenar, April 1993.

NESDIS 66 Catalogue of Heavy Rainfall Cases of Six Inches or more over the Continental U.S. during 1991. Charles Kadin, April 1993.

NESDIS 67 The Relationship between Water Vapor Plumes and Extreme Rainfall Events during the Summer Season. Wassila Thiao, Roderick A. Scofield and Jacob Robinson, May 1993.

NESDIS 68 AMSU-A Engineering Model Calibration. Tsan Mo, Michael P. Weinreb, Norman C. Grody and David Q. Wark, June 1993.

NESDIS 69 Nonlinearity Corrections for the Thermal Infrared Channels of the Advanced Very High Resolution Radiometer: Assessment and Recommendations. C.R. Nagaraja Rao (Editor), June 1993.

NESDIS 70 Degradation of the Visible and Near-Infrared Channels of the Advanced Very High Resolution Radiometer on the NOAA-9 Spacecraft: Assessment and Recommendations for Corrections. C.R. Nagaraja Rao (Editor), June 1993.

NESDIS 71 Spectral Radiance-Temperature Conversions for Measurements by AVHRR Thermal Channels 3,4,5. Paul A. Davis, August 1993.

NESDIS 72 Summary of the NOAA/NESDIS Workshop on Development of a Global Satellite/in Situ Environmental Database. Edited by K.P. Gallo and D.A. Hastings, August 1993.

NESDIS 73 Intercomparison of the Operational Calibration of GOES-7 and METEOSAT-3/4. W. Paul Menzel, Johannes Schmetz, Steve Nieman, Leo Van de Berg, Volker Gaertner, and Timothy J. Schmit, Septmeber 1993.

NOAA SCIENTIFIC AND TECHNICAL PUBLICATIONS

The National Oceanic and Atmospheric Administration was established as part of the Department of Commerce on October 3, 1970. The mission responsibilities of NOAA are to assess the socioeconomic impact of natural and technological changes in the environment and to monitor and predict the state of the solid Earth, the oceans and their living resources, the atmosphere, and the space environment of the Earth.

The major components of NOAA regularly produce various types of scientific and technical information in the following kinds of publications:

PROFESSIONAL PAPERS - Important definitive research results, major techniques, and special investigations.

CONTRACT AND GRANT REPORTS - Reports prepared by contractors or grantees under NOAA sponsorship.

ATLAS - Presentation of analyzed data generally in the form of maps showing distribution of rainfall, chemical and physical conditions of oceans and atmosphere, distribution of fishes and marine mammals, ionospheric conditions, etc.

TECHNICAL SERVICE PUBLICATIONS - Reports containing data, observations, instructions, etc. A partial listing includes data serials; prediction and outlook periodicals; technical manuals, training papers, planning reports, and information serials; and miscellaneous technical publications.

TECHNICAL REPORTS - Journal quality with extensive details, mathematical developments, or data listings.

TECHNICAL MEMORANDUMS - Reports of preliminary, partial, or negative research or technology results, interim instructions, and the like.

U.S. DEPARTMENT OF COMMERCE
National Oceanic and Atmospheric Administration
National Environmental Satellite, Data, and Information Service
Washington, D.C. 20233